



Article

Chemistry of CS₂ and CS₃ Bridged Decaborane Analogues: Regular Coordination Versus Cluster Expansion

Ketaki Kar ¹, Suvam Saha ¹, Rahul Maganbhai Parmar ¹, Arindam Roy ¹, Marie Cordier ², Thierry Roisnel ² 
and Sundargopal Ghosh ^{1,*} 

¹ Department of Chemistry, Indian Institute of Technology Madras, Chennai 600036, India

² Univ Rennes, CNRS, Institut des Sciences Chimiques de Rennes, UMR 6226, F-35000 Rennes, France

* Correspondence: sghosh@iitm.ac.in

Abstract: In an effort to synthesize metallaheteroborane clusters of higher nuclearity, the reactivity of metallaheteroboranes, *nido*–[(Cp**M*)₂B₆S₂H₄(CS₃)] (Cp* = C₅Me₅) (**1**: *M* = Co; **2**: *M* = Rh) with various metal carbonyls have been investigated. Photolysis of *nido*–**1** and *nido*–**2** with group 6 metal carbonyls, M'(CO)₅.THF (*M'* = Mo or W) were performed that led to the formation of a series of adducts [(Cp**M*)₂B₆S₂H₄(CS₃){M'(CO)₅}] (**3**: *M* = Co, *M'* = Mo; **4**: *M* = Co, *M'* = W; **5**: *M* = Rh, *M'* = Mo; **6**: *M* = Rh, *M'* = W) instead of cluster expansion reactions. In these adducts, the S atom of C=S group of di(thioborane)thione {B₂CS₃} moiety is coordinated to M'(CO)₅ (*M* = Mo or W) in η¹-fashion. On the other hand, thermolysis of *nido*–**1** with Ru₃(CO)₁₂ yielded one fused metallaheteroborane cluster [{Ru(CO)₃}₃S{Ru(CO)}{Ru(CO)₂Co₂B₆SH₄(CH₂S₂){Ru(CO)₃}₂S}], **7**. This 20-vertex-fused cluster is composed of two tetrahedral {Ru₃S} and {Ru₂B₂}, a flat butterfly {Ru₃S} and one octadecahedron {Co₂RuB₇S} core with one missing vertex, coordinated to {Ru₂SCH₂S₂} through two boron and one ruthenium atom. On the other hand, the room temperature reaction of *nido*–**2** with Co₂(CO)₈ produced one 19-vertex fused metallaheteroborane cluster [(Cp*Rh)₂B₆H₄S₄{Co(CO)}₂{Co(CO)₂}(μ-CO)S{Co(CO)₃}]₂, **8**. Cluster **8** contains one *nido*–decaborane {Rh₂B₆S₂}, one butterfly {Co₂S₂} and one bicapped square pyramidal {Co₆S} unit that exhibits an intercluster fusion with two sulfur atoms in common. Clusters **3**–**6** have been characterized by multinuclear NMR and IR spectroscopy, mass spectrometry and structurally determined by XRD analyses. Furthermore, the DFT calculations have been carried out to gain insight into electronic, structural and bonding patterns of the synthesized clusters.

Keywords: metallaheteroborane; fusion; coordination; expansion; cluster



Citation: Kar, K.; Saha, S.; Parmar, R.M.; Roy, A.; Cordier, M.; Roisnel, T.; Ghosh, S. Chemistry of CS₂ and CS₃ Bridged Decaborane Analogues: Regular Coordination Versus Cluster Expansion. *Molecules* **2023**, *28*, 998. <https://doi.org/10.3390/molecules28030998>

Academic Editors: Felipe Fantuzzi and Marco A. C. Nascimento

Received: 1 December 2022

Revised: 10 January 2023

Accepted: 13 January 2023

Published: 19 January 2023



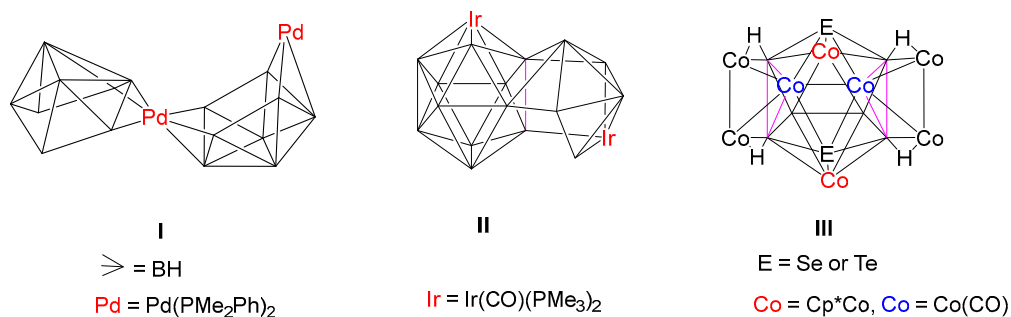
Copyright: © 2023 by the authors. Licensee MDPI, Basel, Switzerland. This article is an open access article distributed under the terms and conditions of the Creative Commons Attribution (CC BY) license (<https://creativecommons.org/licenses/by/4.0/>).

1. Introduction

The chemistry of polyhedral boron clusters has been significantly developed owing to their noteworthy structural appeal exhibited by different coordination modes, unique bonding patterns and their extensive applications in catalysis, material science, boron neutron capture therapy (BNCT), etc [1–7]. Starting with Hawthorne and followed by many main group pioneers such as Lipscomb [8], Grimes [9], Welch [10], Kennedy [11], Fehlner [12,13] and Xie [14], we [15–28] and others [29–31] have reported numerous single cages as well as condensed polyhedral clusters containing boron, chalcogens, carbon and transition metal fragments. Due to the deficiency of the electron octet around boron atom, these clusters display some unusual bonding features with main group elements as well as transition metals [32,33]. Molecular assemblies that involve two or more individual single clusters closely joined together are called fused clusters. Such fused clusters species are known as “macropolyhedral” species that are formed by the fusion of smaller building blocks like tetrahedrons, trigonal bipyramids, octahedra, etc [34–36]. This fusion can occur by sharing common atoms, edges and faces (Chart 1). For example, Kennedy et al., have synthesized **I** from thermal autofusion of [(Pme₂Ph)₂PdB₈H₁₂] [37]. **I** is a vertex-fused cluster which can be contemplated as simple convergence of two starting materials of

arachno {MB₈} geometries. They have also isolated an 18-vertex macropolyhedral diiridaborane(II), comprised of one 12-vertex *closo*-{IrB₁₁} and one 8-vertex *nido*-{IrB₇}, fused by a common {B₂} edge [38]. Successively, we and Fehlner have developed synthetic strategies for the isolation of fused clusters utilizing preformed metallaboranes and monobornes or metal carbonyls [39–43]. For example, the reaction of [(Cp*ReH₂)₂B₄H₄] with [Co₂(CO)₈] led to the formation of a 6 SEP hypoelectronic cluster [(Cp*Re)₂Co₂(CO)₅B₄H₄], in which a 4-electron {Co₂(CO)₅} fragment is coplanar with the B₄ fragment [39]. Fehlner has isolated a hybrid cluster [Fe₂(CO)₆(η⁵-C₅Me₅RuCO)(η⁵-C₅Me₅Ru)B₆H₁₀] from the reaction of *nido*-[(η⁵-C₅Me₅Ru)₂B₆H₁₂] and [Fe₂(CO)₉], in which a {Fe₂B₂} tetrahedron has been fused to ruthenaborane moiety through two common boron atoms [40]. Recently, we have reported an unusual doubly face-fused 16-vertex macropolyhedral cluster, [(Cp*Co)₂B₆H₆E₂{Co₂(CO)₂}(μ-CO)₂{Co₄(CO)₈}] (E = Se or Te), III which can be described as a fusion of three individual polyhedral such as the two 5-vertex *nido*-square pyramid {Co₃B₂} and one 12-vertex icosahedron {Co₄B₆E₂} units having two common triangular faces [43].

Cluster Expansion



Coordination

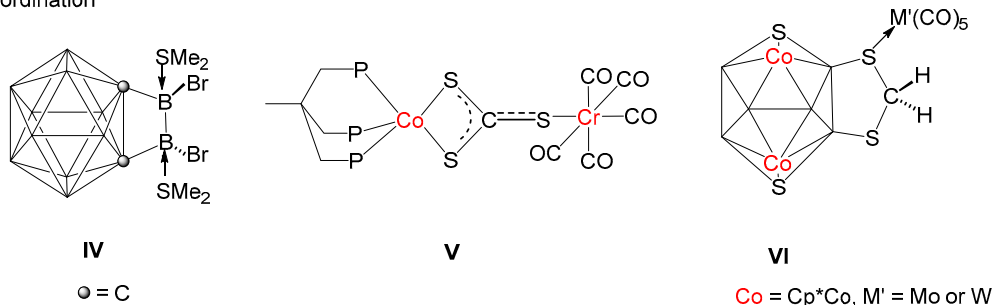


Chart 1. Different types of cluster expansion and coordination.

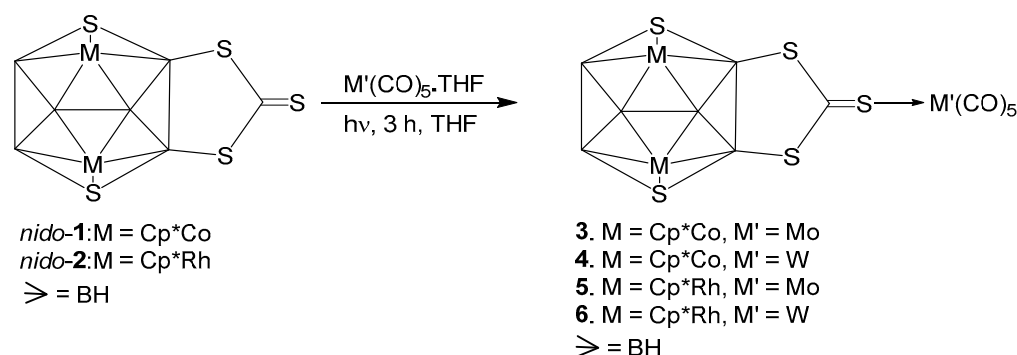
Apart from cluster fusion, several coordination compounds have been synthesized involving metal carbonyl fragments, chalcogens, boranes, and metallaboranes following the same way [44–46]. Beginning from the synthesis of [Pt(CS₂)(PPh₃)₂], the first CS₂ metal complex by Wilkinson and co-workers, a range of CS₂ complexes containing transition metals have been synthesized [47]. Transition metal-{S₂CS} moiety can act as a ligand to bind to one or two metal centres [48]. As shown in Chart 1, Zouwei Xie and co-workers have reported [1,2-{BBrSMe₂}]₂-*o*-C₂B₁₀H₁₀] (IV) in which Sme₂ groups are coordinated to *exo*-boron atoms [49]. Bianchini et al., have reported complex V in which two sulfur atoms are connected to Co, whereas the third sulfur atom of {CS₃} unit is linked to a Cr(CO)₅ fragment through a σ bond [50]. Recently, we have isolated [(Cp*Co)₂B₆S₂H₄(CH₂S₂)]{M'(CO)₅} (VI, M' = Mo, W) from the photolysis of {CH₂S₂} bridged decaborane-14 analogue *nido*-[(Cp*Co)₂B₆S₂H₄(CH₂S₂)] with {M'(CO)₅·THF} (M' = Mo or W) fragments [42]. The molecular structure of VI shows that one of the sulfur atoms of the {CH₂S₂} moiety is coordinated to {M'(CO)₅} (M' = Mo or W) in η^1 -fashion. However, when *nido*-[(Cp*Co)₂B₆S₂H₄(CH₂S₂)] was treated with [Fe₂(CO)₉] at room temperature, it afforded an 11-vertex *nido*-[(Cp*Co)₂B₆S₂H₄(CH₂S₂)]{Fe(CO)₃}, which is similar to [C₂B₉H₁₁]²⁻ with a five-

membered pentahapto coordinating face [43]. Along with *nido*-[(Cp*Co)₂B₆S₂H₄(CH₂S₂)], we also have isolated CS₃ bridged decaborane-14 analogues, *nido*-[(Cp*M)₂B₆S₂H₄(CS₃)] (1: M = Co; 2: M = Rh) [42]. Based on the computational studies, it was proposed that clusters *nido*-1 and *nido*-2 have the ability to attract electrophiles as well as nucleophiles. Thus, in order to validate our theoretical assumptions, we have investigated the reactivity of *nido*-1 and *nido*-2 with different metal carbonyls such as M'(CO)₅.THF (M' = Mo or W), Ru₃(CO)₁₂ and Co₂(CO)₈ that afforded coordination compounds as well as higher-vertex fused macropolyhedral clusters with unusual bonding.

2. Results and Discussion

2.1. Reactivity of *nido*-1 and *nido*-2 with M'(CO)₅.THF (M = Mo, W)

As shown in Scheme 1, photolysis of *nido*-1 with M'(CO)₅.THF (M' = Mo or W) produced adducts [(Cp*Co)₂B₆S₂H₄(CS₃){M'(CO)₅}] (3: M' = Mo; 4: M' = W) as violet and red solids, respectively (Scheme 1). These compounds were characterized by ¹H{¹¹B}, ¹¹B{¹H}, and IR spectroscopy along with ESI mass spectrometry. The ¹H{¹¹B} NMR spectra of 3 and 4 exhibit the existence of single Cp* environments appearing at δ = 1.65 and 1.69 ppm, respectively. The ¹¹B{¹H} NMR spectra of 3 and 4 display four resonances appeared at δ = 26.5, 27.6, 33.0 and 37.7 ppm (for 3) and δ = 24.6, 26.4, 33.4 and 38.2 ppm (for 4). However, the identity was unclear until an X-ray crystallographic analysis was carried out for one of them. Despite of our several attempts, we could not get good quality crystals for 3. The CH₂Cl₂-hexane solution of 4 at −5 °C yielded X-ray quality crystals that allowed us to study the X-ray diffraction of 4.



Scheme 1. Synthesis of metal carbonyl coordinated clusters 3, 4, 5 and 6.

The solid-state X-ray structure of 4, shown in Figure 1, reveals that the S atom of C=S group of di(thioborane)-thione {B₂CS₃} moiety is coordinated to W(CO)₅ in η¹-fashion. The S1-C1 bond distance of 1.648(12) Å in 4 is slightly longer than C=S bond length of *nido*-1 [1.636(6) Å]. The W-S bond distance of 4 [W1-S1 2.529 (3) Å] is slightly longer compared to [CpW(CO)₂{η²-(S₂CC₆H₄Me₄)}] (2.472 Å) [51]. This may be due to the effect of monodentate ligation of {CS₃} to W atom. Deliberating the spectroscopic data of 3 and 4 along with the X-ray structure of 4, it is reasonable to assume that 3 is a Mo analogue of 4.

Similarly, compounds 5 and 6 were synthesized from the reaction of *nido*-2 with M'(CO)₅.THF (M' = Mo or W) at photolytic conditions, respectively. The ¹H{¹¹B} NMR spectra of 5 and 6 exhibit the existence of single Cp* environments appearing at δ = 1.85 and 1.80 ppm, respectively. The ¹¹B{¹H} NMR spectra of 5 and 6 show four resonances each appeared at δ = 17.3, 20.3, 24.6 and 30.4 ppm (for 5) and δ = 16.7, 20.5, 23.9 and 24.9 ppm (for 6). All these spectroscopic data of 5 and 6 suggest that they are analogous to 3 and 4, respectively. In order to confirm this assumption, the single-crystal X-ray structure analyses of suitable crystals of 5 and 6 were undertaken. As shown in Figure 2, the solid-state structures of 5 and 6 display that S atom of C=S group of di(thioborane)-thione {B₂CS₃} moiety is coordinated to M'(CO)₅ (M' = Mo or W) in η¹-fashion. The C=S bond distance of 1.668(6) Å in 5 and 1.672 (3) Å in 6 are slightly longer than the C=S bond length of *nido*-2 [1.635(9) Å]. The M'-S bond distances of 5 [Mo1-S5 2.539 (15) Å] and 6 [W1-S5 2.293 (7)

Å] are slightly longer compared to those of $[\text{CpMo}(\text{CO})_2\{\eta^2-(\text{S}_2\text{CCH}_2^t\text{Bu})\}]$ (2.477 Å) and $[\text{CpW}(\text{CO})_2\{\eta^2-(\text{S}_2\text{CC}_6\text{H}_4\text{Me}_4)\}]$ (2.472 Å), respectively.[52] This may be due to the effect of monodentate ligation of $\{\text{CS}_3\}$ to Mo or W atoms.

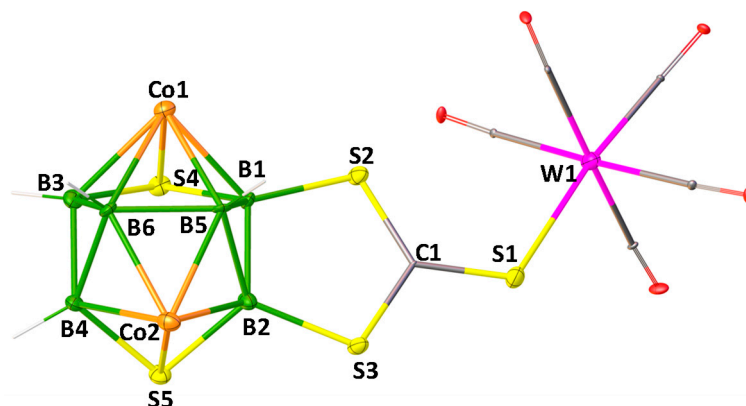


Figure 1. Molecular structure and labelling diagram of **4** (note that Cp^* ligands attached to metals are omitted for clarity). Selected bond lengths (Å) and angles ($^\circ$): **4**: B1–B2 1.790(19), W1–S1 2.529(3), S1–C1 1.648(12), S2–B1 1.886(12); C1–S1–W1 116.3(4), C1–S2–B1 102.0(6).

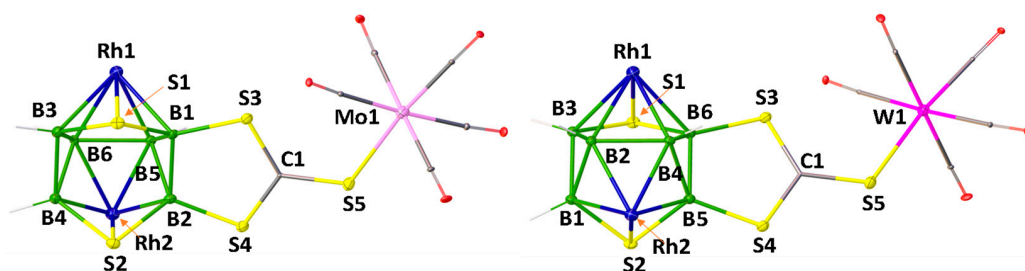


Figure 2. Molecular structures and labelling diagrams of **5** and **6** (note that Cp^* ligands attached to metals are omitted for clarity). Selected bond lengths (Å) and angles ($^\circ$): **5**: B1–B2 1.808(8), Mo1–S5 2.5388(15), S5–C1 1.668(6), S3–B1 1.869(6); C1–S5–Mo1 117.1(2), C1–S3–B1 101.1(3). **6**: B5–B6 1.809(4), W1–S5 2.5293(7), S5–C1 1.672(3), S3–B6 1.873(3); C1–S5–W1 116.73(9), C1–S3–B6 101.03(12).

To provide some insight into the electronic structures and bonding relationship of the adducts **3–6**, the DFT calculations using the Gaussian 16 program with a BP86/def2-svp level of theory have been carried out. The MO analysis, shown in Figure 3, shows that the HOMO-LUMO gap for **3**, in which the $[\text{Mo}(\text{CO})_5]$ moiety is coordinated to C=S group of di(thioborane)-thione $\{\text{B}_2\text{CS}_3\}$ is more as compared to its tungsten analogue **4**. The similar trend has been observed in case of **5** and **6**. However, the HOMO-LUMO gap for the Rh systems (**5** and **6**) is greater than the Co systems (**3** and **4**). The highest HOMO-LUMO gap is observed for compound **5**, which indirectly indicates higher stability than its Co analogue.

2.2. Condensed Clusters: $[\{\text{Ru}(\text{CO})_3\}_3\text{S}\{\text{Ru}(\text{CO})\}\{\text{Ru}(\text{CO})_2\}\text{Co}_2\text{B}_6\text{SH}_4\{\text{Ru}(\text{CO})_3\}_2(\text{SCH}_2\text{S}_2)]$, **7** and $[(\text{Cp}^*\text{Rh})_2\text{B}_6\text{H}_4\text{S}_4\{\text{Co}(\text{CO})\}_2\{\text{Co}(\text{CO})_2\}_2(\mu\text{-CO})\text{S}\{\text{Co}(\text{CO})_3\}_2]$, **8**

Although the reactions of *nido-1* and *nido-2* with group 6 metal carbonyls yielded simple coordination compounds, reactions with both $\text{Ru}_3(\text{CO})_{12}$ and $\text{Co}_2(\text{CO})_8$ led to the formation of condensed clusters $[\{\text{Ru}(\text{CO})_3\}_3\text{S}\{\text{Ru}(\text{CO})\}\{\text{Ru}(\text{CO})_2\}\text{Co}_2\text{B}_6\text{SH}_4\{\text{Ru}(\text{CO})_3\}_2(\text{SCH}_2\text{S}_2)]$ **7** and $[(\text{Cp}^*\text{Rh})_2\text{B}_6\text{H}_4\text{S}_4\{\text{Co}(\text{CO})\}_2\{\text{Co}(\text{CO})_2\}_2(\mu\text{-CO})\text{S}\{\text{Co}(\text{CO})_3\}_2]$ **8**, respectively (Scheme 2). Note that, both these clusters were isolated in very poor yields which were merged with unreacted precursors *nido-1* and *nido-2* while doing thin-layered chromatography (TLC). Although we were not able to purify them, fractional crystallization allowed us to get a few crystals of them for X-ray diffraction studies. Therefore, the characterization of both **7** and **8** are solely based on the molecular structures obtained from the single crystal XRD analysis.

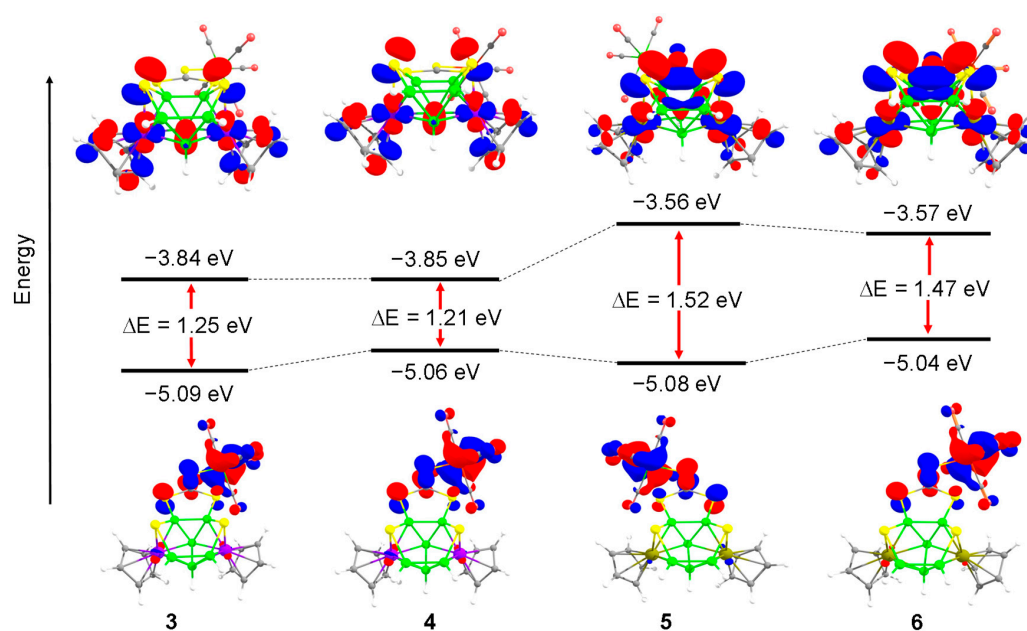
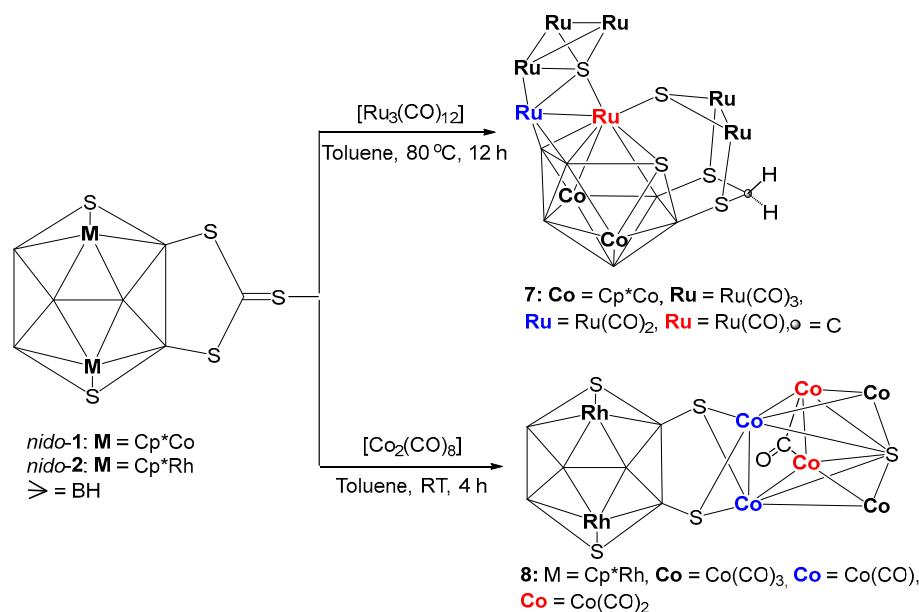


Figure 3. Comparison of frontier molecular orbitals of **3**, **4**, **5** and **6**; respectively. Contour values for isosurface are ± 0.04 (e/bohr^3) $^{1/2}$.



Scheme 2. Synthesis of fused clusters **7** and **8**.

2.2.1. Structural Account of 7

As shown in Figure 4a, the molecular structure of **7** reveals the molecular formula as $[\{\text{Ru}(\text{CO})_3\}_3\text{S}\{\text{Ru}(\text{CO})\}\{\text{Ru}(\text{CO})_2\}\text{Co}_2\text{B}_6\text{SH}_4\{\text{Ru}(\text{CO})_3\}_2(\text{SCH}_2\text{S}_2)]$. This is a 20-vertex macro-polyhedral metallaheteroborane cluster, in which fusion and coordination are observed concurrently (Figure 4a). The cluster **7** comprises of two tetrahedral clusters $\{\text{Ru}_3\text{S}\}$ and $\{\text{Ru}_2\text{B}_2\}$, one butterfly $\{\text{Ru}_3\text{S}\}$, one missing vertex octadecahedron $\{\text{Co}_2\text{B}_6\text{RuS}\}$ and one exopolyhedral moiety $\{\text{Ru}_2\text{SCH}_2\text{S}_2\}$. Tetrahedron $\{\text{Ru}_3\text{S}\}$ unit and butterfly $\{\text{Ru}_3\text{S}\}$ unit are fused by one common $\{\text{Ru}-\text{S}\}$ edge. The butterfly $\{\text{Ru}_3\text{S}\}$ unit is fused through a common $\{\text{Ru}-\text{Ru}\}$ edge with another tetrahedral $\{\text{Ru}_2\text{B}_2\}$, fused with one missing vertex octadecahedron $\{\text{Co}_2\text{B}_6\text{RuS}\}$ with a common triangular $\{\text{RuB}_2\}$ face. The exopolyhedral moiety $\{\text{Ru}_2\text{SCH}_2\text{S}_2\}$ is coordinated to Ru5, B6 and B5 atoms of *nido*- $\{\text{Co}_2\text{B}_6\text{RuS}\}$ subcluster through its S2, S4 and S5 atoms, respectively (Figure 4b). In other way, we can explain

that S2, S4 and S5 atoms of $\{\text{Ru}_2\text{S}(\text{CH}_2\text{S}_2)\}$ unit bridge to Ru5, B6 and B5 atoms of *nido*- $\{\text{Co}_2\text{B}_6\text{RuS}\}$ unit, respectively in *exo* fashion. Additionally, the butterfly $\{\text{Ru}_3\text{S}\}$ unit of **7** is almost flat with a dihedral angle of 172.93° (Figure 4a). Although there are few instances of tetrametallic butterfly clusters that are flattened or almost flattened, flat butterfly clusters containing transition metal and main group vertices are exceptional [52]. The ruthenium-sulfur bond lengths in $\{\text{Ru}_3\text{S}\}$ butterfly core of **7** (avg. 2.489 Å) are considerably longer than the bond length of $[(\text{Cp}^*\text{Ru})_2(\mu, \eta^3\text{-CHS})_2]$ (2.3733 Å) [53,54].

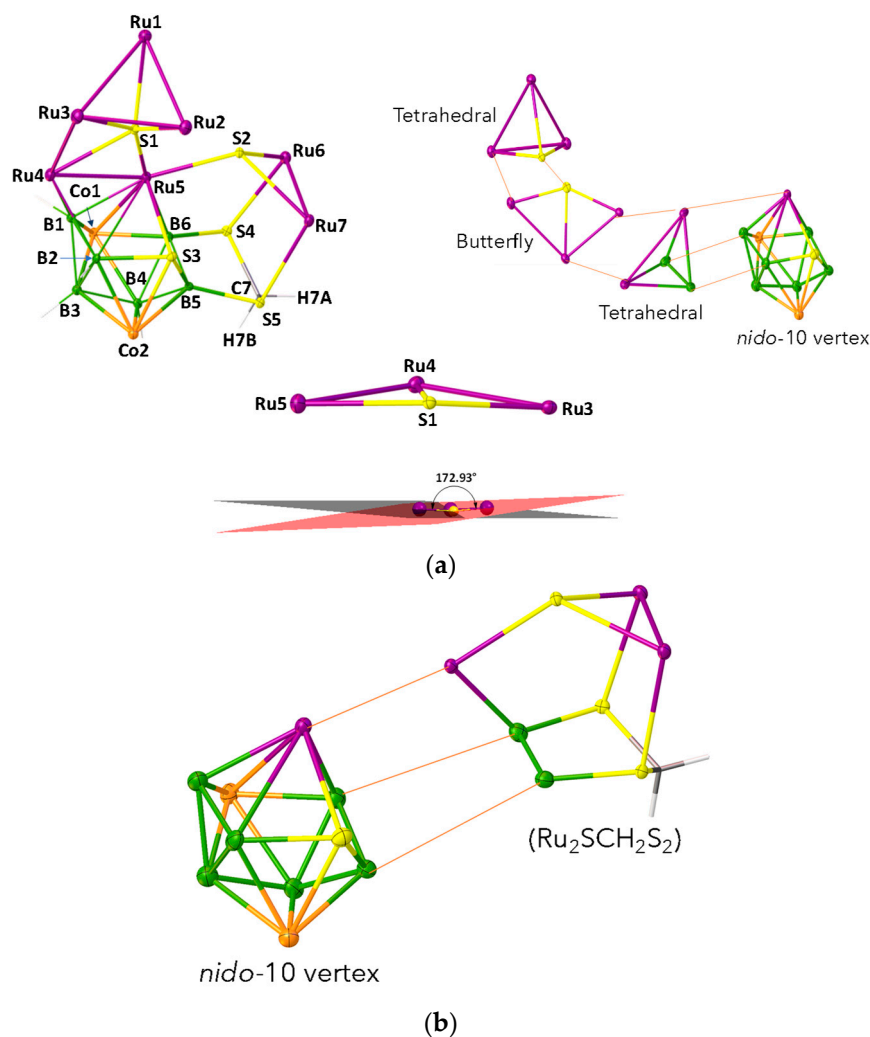


Figure 4. (a) Molecular structure, labelling diagram (**left**), fusion demonstration (**right**) and demonstration with dihedral angles between planes of Ru5-S1-Ru4 and Ru4-S1-Ru3 triangles of $\{\text{Ru}_3\text{S}\}$ butterfly subcluster (**bottom**), of **7** (note that Cp^* ligands and carbonyl groups attached to metals are omitted for clarity). Selected bond lengths (Å) and angles ($^\circ$): **7**: Ru1-S1 2.3488(18), Ru3-S1 2.4798(18), Ru4-S1 2.5153(18), Ru3-Ru4 3.0572(8), Ru7-S2 2.4311(17), S5-C7 1.821(7); Ru5-S1-Ru3 $145.51(8)$, Ru4-S1-Ru3 $75.47(5)$. (b) Fusion of *nido*-10 vertex $\{\text{Co}_2\text{B}_6\text{RuS}\}$ and $\{\text{Ru}_2\text{SCH}_2\text{S}_2\}$ cores of **7**. (Cp^* ligands and carbonyl groups attached to metals are omitted for clarity).

The HOMO of **7** exhibits the π -bonding interactions among the d orbitals of three Ru atoms and p orbital of one sulfur atom of the $\{\text{Ru}_3\text{S}\}$ tetrahedron core. On the other hand, the σ -antibonding interactions between the Co, Ru (d orbitals) and S atom (p orbital) of the *nido*- $\{\text{Co}_2\text{B}_6\text{RuS}\}$ core was observed in LUMO of **7** (Figure 5). The HOMO-28 shows an extended overlap of the d orbitals of three Ru atoms of the $\{\text{Ru}_3\text{S}\}$ tetrahedron indicating a trimetallic-bonding scenario (Figure 5). The presence of localised non-bonding p orbitals on S2 and S5 atoms observed in HOMO-4 (Figure 5) and HOMO-36 (Figure S23) makes **7** a suitable candidate for further cluster growth reactions.

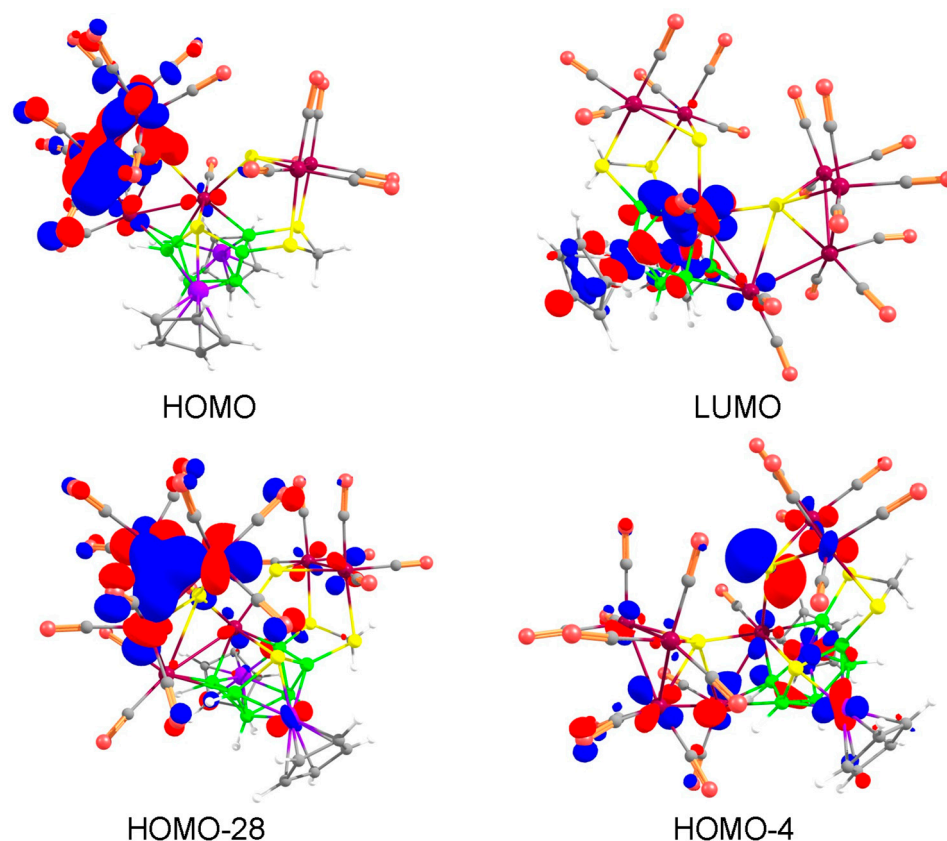


Figure 5. Key frontier molecular orbitals of **7**. Contour values for isosurface are ± 0.04 (e/bohr^3)^{1/2}.

2.2.2. Structural Account of **8**

As shown in Figure 6, the X-ray structure of **8** shows the molecular formula as $[(\text{Cp}^*\text{Rh})_2\text{B}_6\text{H}_4\text{S}_4\{\text{Co}(\text{CO})\}_2\{\text{Co}(\text{CO})_2\}_2(\mu\text{-CO})\text{S}\{\text{Co}(\text{CO})_3\}_2]$. Although, this looks like a fusion of three polyhedra, for example, one bicapped square pyramid $\{\text{Co}_6\text{S}\}$, one butterfly $\{\text{Co}_2\text{S}_2\}$ and one 10 vertex *nido*- $\{\text{Rh}_2\text{B}_6\text{S}_2\}$, careful evaluation of this cluster shows that one bicapped square pyramidal $\{\text{Co}_6\text{S}\}$ core is fused with a butterfly $\{\text{Co}_2\text{S}_2\}$ unit via one common $\{\text{Co}_2\}$ edge. This entire fused cluster $\{\text{S}_2\text{Co}_6\text{S}\}$ is coordinated to B4 and B6 atoms of 10 vertex *nido*- $\{\text{Rh}_2\text{B}_6\text{S}_2\}$ through the wingtip S3 and S4 atoms of the butterfly $\{\text{Co}_2\text{S}_2\}$.

The structural account of **8** can also be described in a different approach. As shown in Figure 7, this may be considered as two intercluster crosslinks, in which two sulfur atoms (S3 and S4) are bridged by two Co1 and Co2 atoms of the bicapped square pyramidal $\{\text{Co}_6\text{S}\}$ and two boron atoms (B4 and B6) on the 10-vertex *nido*- $\{\text{Rh}_2\text{B}_6\text{S}_2\}$ subcluster in μ^3 -fashion. A similar description has also been proposed for $[(\text{PPh}_3)\text{NiS}_2\text{B}_{16}\text{H}_{12}(\text{PPh}_3)]$ by Kennedy [55]. As shown in Figure 7, in case of **A**, there is an intercluster crosslink in which a sulfur atom bridges two boron atoms of the 9-vertex *nido*- $\{\text{NiB}_8\}$ subcluster and a boron atom on the 12-vertex *closo*- $\{\text{NiSB}_{10}\}$ subcluster in μ^3 fashion.

As shown in Figure 8, the MO analysis of cluster **8** reveals that the HOMO consists of mainly the d orbitals of cobalt atoms of $\{\text{Co}_6\text{S}\}$ core, whereas the non-bonding p-orbitals of the wingtip S3 and S4 atoms of the butterfly $\{\text{Co}_2\text{S}_2\}$ contribute to the LUMO. The HOMO-11 displays an antibonding interaction between Rh1 and S1 as well as Rh2 and S2, that make the Rh1-S1 and Rh2-S2 bonds susceptible for nucleophilic attack. On the other hand, the HOMO-32 reveals conjugated π -interactions in both Co2-Co5-Co7 and Co1-Co5-Co6 planes of the bicapped square pyramidal $\{\text{Co}_6\text{S}\}$ unit (Figure 8). This leads us to presume that these two planes are prone to electrophilic substitution. In addition, HOMO-35 displays orbital overlap between two cobalt atoms and two sulfur atoms of the $\{\text{Co}_2\text{S}_2\}$ butterfly fragment (Figure S24 in Supplementary Materials).

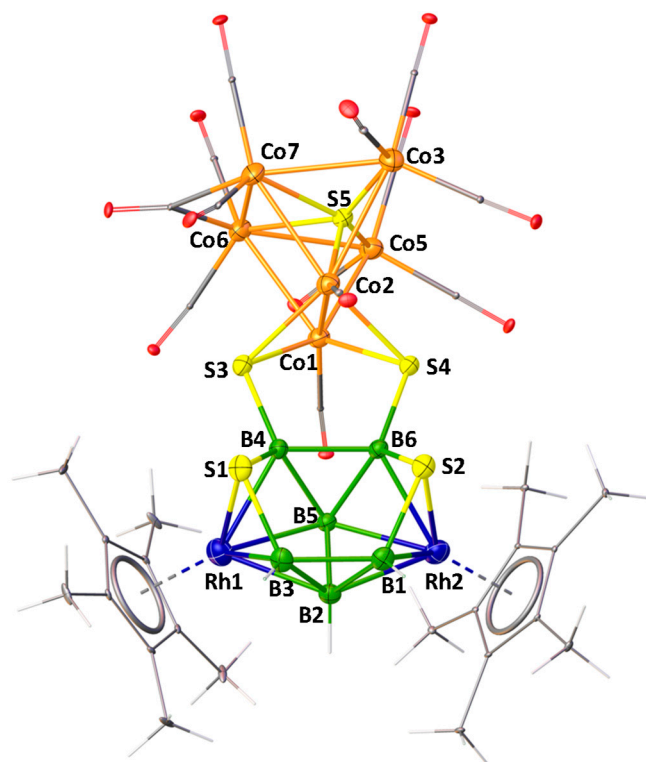


Figure 6. Molecular structure and labelling diagram of **8**. Selected bond lengths (Å) and angles (°). **8**: Co1–Co2 2.4288(6), Co1–S5 2.2790(8), Co1–Co6 2.5962(5), Co6–Co7 2.6164(7), B4–S3 1.868(3), Co1–S3 2.2313(9); Co1–S5–Co2 64.63(2), Co3–S5–Co5 137.88(4).

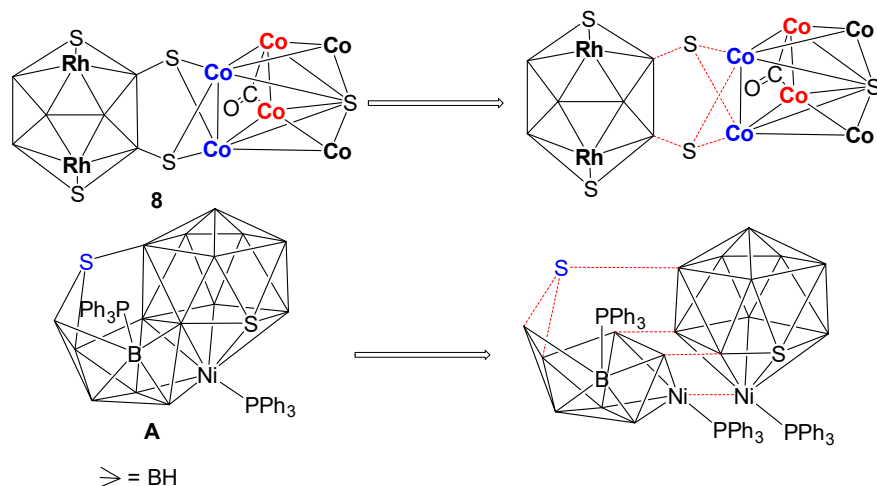


Figure 7. Representation of intercluster crosslink in clusters **8** and $[(\text{PPh}_3)\text{NiS}_2\text{B}_{16}\text{H}_{12}(\text{PPh}_3)]$.

In order to understand the geometries of many main groups as well as transition metal-fused clusters, cluster electron-counting rules [56–59] are now well established as conceptual and practical tools. However, both clusters **7** and **8** do not follow any of the cluster-counting rules, including Mingos' fusion formalism [58] and Jemmis' mno rule [59]. The electron counts are very complex for both **7** and **8**. This may be due to the fact that these clusters contain multiple fragments and several metal–metal bonds.

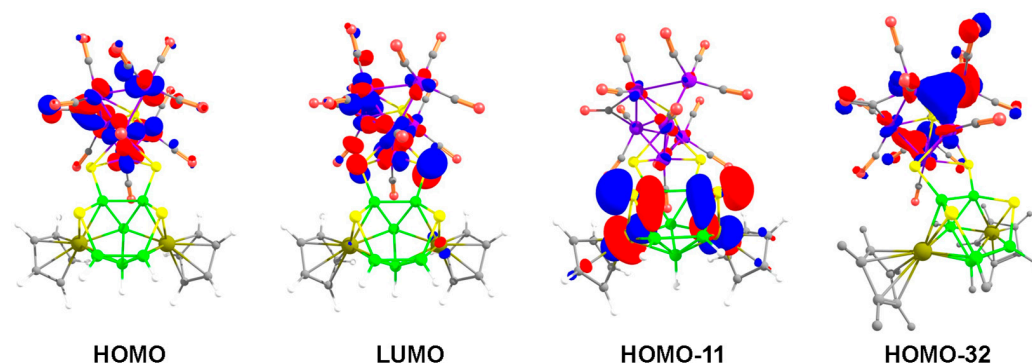


Figure 8. Key frontier molecular orbitals of **8**. Contour values for isosurface are ± 0.04 (e/bohr^3)^{1/2}.

3. Experimental Section

3.1. Materials and Methods

All the manipulations were accomplished in argon atmosphere using schlenk line techniques or inside the glove box. Dichloromethane, Hexane, Toluene, and THF were distilled by using appropriate drying agents (Na/benzophenone) in argon atmosphere prior to use. All chemicals, such as $[\text{Co}_2(\text{CO})_8]$, $[\text{Ru}_3(\text{CO})_{12}]$, $[\text{Mo}(\text{CO})_6]$, $[\text{W}(\text{CO})_6]$, LiBH_4 (2.0 M in THF) were used as purchased from Sigma Aldrich. The starting materials *nido*- $[(\text{Cp}^*\text{M})_2\text{B}_6\text{S}_2\text{H}_4(\text{CS}_3)]$ ($\text{Cp}^* = \eta^5\text{-C}_5\text{Me}_5$, **1**: M = Co, **2**: M = Rh) were synthesized according to the literature procedures [42]. All the syntheses detailed here are reproducible. To separate reaction mixtures, aluminium-supported TLC plates (MERCK) of 250 μm diameter were used. Some 400 and 500 MHz Bruker FT-NMR spectrometers were used to record $^1\text{H}\{^{11}\text{B}\}$ and $^{11}\text{B}\{^1\text{H}\}$ NMR spectra. The residual solvent protons (CDCl_3 , $\delta = 7.26$ ppm) were employed as a reference the ^1H NMR spectra, respectively. The ESI-MS spectra were recorded in a Bruker MicroTOF-II mass spectrometer. The infrared spectra (IR) were recorded using JASCO FT/IR-1400 spectrometer.

3.2. Formation of **3** and **4**

In a flame-dried Schlenk tube under an Ar atmosphere, previously reported *nido*-**1** (0.03 g, 0.048 mmol) was suspended in 5 mL of dry THF at room temperature. A freshly prepared solution of $[\text{Mo}(\text{CO})_5\cdot\text{THF}]$ from the photolysis of $\text{Mo}(\text{CO})_6$ (0.012 g, 0.048 mmol) in THF (5 mL) was added dropwise to the yellow solution of *nido*-**1**. The reaction mixture was irradiated for 3 h, and we observed the color change from yellow to reddish brown. The solvent was removed in the vacuum. Then, the residue was extracted with n-hexane and filtered through 3 cm of celite. The reaction mixture was purified on TLC plates. Elution with a CH_2Cl_2 /n-hexane (30:70 v/v) mixture afforded a violet solid **3** (2.9 mg, 7%). In the same reaction conditions, treatment of *nido*-**1** with $[\text{W}(\text{CO})_5\cdot\text{THF}]$ prepared from the photolysis of $\text{W}(\text{CO})_6$ (0.016 g, 0.048 mmol) in THF (5 mL), yielded a red solid **4** (4.14 mg, 9%).

Spectroscopic data of **3**: $^{11}\text{B}\{^1\text{H}\}$ NMR (160 MHz, C_6D_6 , 22 °C): δ (ppm) = 26.5 (br, 2B), 27.6 (br, 2B), 33.0 (br, 1B), 37.7 (br, 1B); ^1H NMR (500 MHz, CDCl_3 , 22 °C): δ (ppm) = 1.65 (s, 15H; $1 \times \text{Cp}^*$), IR (dichloromethane, cm^{-1}): $\bar{\nu}$ = 2418 (B-H_t), and 1941 (terminal CO).

Spectroscopic data of **4**: MS (ESI⁺): calcd for $[\text{C}_{26}\text{H}_{34}\text{B}_6\text{Co}_2\text{O}_5\text{S}_5\text{W}]^+$: m/z 953.9741, found: 953.9784; $^{11}\text{B}\{^1\text{H}\}$ NMR (160 MHz, CDCl_3 , 22 °C): δ (ppm) = 24.6 (br, 2B), 26.4 (br, 1B), 33.4 (br, 2B), 38.2 (br, 1B); ^1H NMR (500 MHz, CDCl_3 , 22 °C): δ (ppm) = 1.69 (s, 15H; $1 \times \text{Cp}^*$); $^1\text{H}\{^{11}\text{B}\}$ NMR (500 MHz, CDCl_3 , 22 °C): 3.49 (br, 1H, BH_t), 3.75 (s, 2H, BH_t), 4.03 (s, 1H, BH_t); IR (dichloromethane, cm^{-1}): $\bar{\nu}$ = 2477 (B-H_t), and 1923 (terminal CO).

3.3. Formation of **5** and **6**

In a flame-dried Schlenk tube under an Ar atmosphere, *nido*-**2** (0.02 g, 0.0278 mmol) was suspended in 5 mL of dry THF at room temperature. A freshly prepared solution of $[\text{Mo}(\text{CO})_5\cdot\text{THF}]$ from the photolysis of $\text{Mo}(\text{CO})_6$ (0.007 g, 0.0278 mmol) in THF (5 mL),

was added dropwise to the yellow solution of *nido-2*. The reaction mixture was irradiated for 3 h, the color changed from yellow to reddish brown. The solvent was removed in the vacuum. Then, the residue was extracted with *n*-hexane and filtered through 3 cm of celite. The reaction mixture was purified on TLC plates. Elution with a CH₂Cl₂/*n*-hexane (30:70 *v/v*) mixture afforded an orange solid **5** (2.16 mg, 8%). In the same reaction conditions, treatment of *nido-2* with [W(CO)₅·THF] prepared from the photolysis of W(CO)₆ (0.009 g, 0.0278 mmol) in THF (5 mL), yielded a red solid **6** (2.94 mg, 10%).

Spectroscopic data of **5**: MS (ESI⁺): calcd for [C₂₆H₃₄B₆Rh₂S₅MoO₅ – (Mo(CO)₅) + H]⁺: *m/z* 719.0010, found: 719.0036; ¹¹B{¹H} NMR (160 MHz, CDCl₃, 22 °C): δ (ppm) = 17.3 (br, 2B), 20.3 (br, 1B), 24.6 (br, 2B), 30.4 (br, 1B); ¹H NMR (500 MHz, CDCl₃, 22 °C): δ (ppm) = 1.85 (s, 15H; 1 × Cp^{*}); ¹H{¹¹B} NMR (500 MHz, CDCl₃, 22 °C): 3.50 (br, 1H, BH_t), 3.75 (s, 2H, BH_t), 4.06 (s, 1H, BH_t); IR (dichloromethane, cm^{−1}): $\bar{\nu}$ = 2403 (B–H_t), 1941 (terminal CO).

Spectroscopic data of **6**: MS (ESI⁺): calcd for [C₂₆H₃₄B₆Rh₂S₅WO₅ + NH₄]⁺: *m/z* 1059.9531, found: 1059.9754 ¹¹B{¹H} NMR (160 MHz, C₆D₆, 22 °C): δ (ppm) = 16.7 (br, 2B), 20.5 (br, 1B), 23.9 (br, 2B), 24.9 (br, 1B); ¹H NMR (500 MHz, CDCl₃, 22 °C): δ (ppm) = 1.80 (s, 15H; 1 × Cp^{*}), ¹H{¹¹B} NMR (500 MHz, CDCl₃, 22 °C): 4.67 (br, 1H, BH_t), 4.75 (s, 1H, BH_t), 5.09 (s, 2H, BH_t); IR (dichloromethane, cm^{−1}): $\bar{\nu}$ = 2453 (B–H_t), 1925 (terminal CO).

3.4. Formation of Metallaheteroborane 7

In a flame-dried Schlenk tube, under argon atmosphere, a yellow solution of *nido-1* (0.03 g, 0.048 mmol) in 10 mL dry toluene was charged with [Ru₃(CO)₁₂] (0.061 g, 0.096 mmol) at room temperature. The reaction mixture was stirred for additional 16 h at 80 °C. The solvent was removed under vacuum and the residue was extracted into hexane/CH₂Cl₂ (70:30 *v/v*) mixture and passed through Celite. Note that compound **7** was isolated in very poor yield and it was combined with the unreacted precursor *nido-1* in thin-layered chromatography (TLC). As a result, purification of **7** was not possible for spectroscopic characterization. Although we were not able to purify it, the fractional crystallization allowed us to get few crystals of **7** for X-ray diffraction studies.

3.5. Formation of Metallaheteroborane 8

Under argon atmosphere, in a flame-dried Schlenk tube, the yellow solution of *nido-2* (0.02 g, 0.0278 mmol) in dry toluene (10 mL) was charged dropwise with a solution of [Co₂(CO)₈] (0.019 g, 0.0556 mmol) in 5 mL dry toluene at room temperature for 16 h. The colour of the reaction mixture was changed from yellow to deep brown. The solvent was removed under vacuum and the residue was extracted into hexane/CH₂Cl₂ (70:30 *v/v*) mixture and passed through celite. Compound **8** was isolated in very poor yield that was merged with unreacted precursor *nido-2* in thin-layered chromatography (TLC). Thus, the purification of **8** for spectroscopic data was not possible. Although we were not able to purify it, fractional crystallization allowed us to get few crystals of **8** for X-ray diffraction studies.

3.6. X-ray Structure Determination

Suitable crystals of **4**, **5**, **6**, **7** and **8** were grown at −5 °C by slow diffusion of a CH₂Cl₂-hexane solution. The X-ray data were collected and integrated by using D8 VENTURE Bruker AXS for **4**, **5**, **6** and **7** with a CMOS-PHOTON70 detector having multilayer device monochromated Mo-Kα (λ = 0.71073 Å) radiation at 150(2) K. For **8**, the X-ray data were collected and integrated by using Bruker D8 VENTURE diffractometer with PHOTON II detector having graphite monochromated Mo-Kα (λ = 0.71073 Å) radiation at 297(2) K. Using SHELXT-2014, SHELXS-97, [60,61] the structures were solved and using SHELXL-2014, SHELXL-2017, SHELXL-2018, and in [62] the structures were refined. For **5**, The contribution of the disordered solvents to the calculated structure factors was estimated following the BYPASS algorithm [63], implemented as the SQUEEZE option in PLATON [64]. A new data set, free of solvent contribution, was then used in the final refinement. All non-Hydrogen atoms were refined with anisotropic atomic displacement parameters. Ex-

cept Hydrogen atoms linked to Boron atoms that were introduced in the structural model through Fourier difference maps analysis, H atoms were finally included in their calculated positions and treated as riding on their parent atom with constrained thermal parameters. For **8**, due to the highly disordered nature of cyclopentadienyl moieties, SHELXL restraint, RIGU, had to be used to impose physically reasonable relative motion of the atoms. It restrains the anisotropic displacement parameters of bonded atoms to be similar along the bond. A PLATON/check cif indicated that there are solvent accessible voids in the lattice. However, the solvent (CH_2Cl_2) could not be modelled from difference electron density peaks. Hence, it was decided to squeeze the electron densities corresponding to the disordered solvent molecules. PLATON/SQUEEZE [65] (Version = 10719) program was used to find out solvent accessible volume and electron counts. A total number of 73 electrons were found in the void with a solvent accessible volume of 439 \AA^3 , which corresponds to 16% of the unit cell volume. Without solvent molecules $R_1 = 0.033$ for 10153 reflections of $F_o > 4\text{sig}(F_o)$ and $wR_2 = 0.1078$ for all data. With solvent contribution (SQUEEZE) $R_1 = 0.029$ for 10145 reflections of $F_o > 4\text{sig}(F_o)$ and $wR_2 = 0.076$ for all data. All the structures of the clusters were drawn using Olex2 [66]. The Cambridge Crystallographic Data Center has been provided with the crystallographic data of the molecules as supplementary publications no CCDC- 2211791 (**4**), 2211792 (**5**), 2214567 (**6**), 2214528 (**7**), and 2144409 (**8**) contain crystallographic data. These data can be obtained free of charge from the Cambridge Crystallographic Data Centre via www.ccdc.cam.ac.uk/data_request/cif (accessed on 7 October 2022).

Crystal data of **4**. $\text{C}_{26}\text{H}_{34}\text{B}_6\text{Co}_2\text{O}_5\text{S}_5\text{W}$, formula weight, $M_r = 953.40$, Monoclinic, $P 2_1/c$, unit cell, $a = 15.603(2) \text{ \AA}$, $b = 17.630(2) \text{ \AA}$, $c = 15.3019(19) \text{ \AA}$, $\alpha = 90^\circ$, $\beta = 118.175(4)^\circ$, $\gamma = 90^\circ$; $Z = 4$; $V = 3710.5(8) \text{ \AA}^3$; $\mu = 4.291 \text{ mm}^{-1}$; $F(000) = 1872$; $\rho_{\text{calcd}} = 1.707 \text{ g/cm}^3$; $R_1 = 0.0735$; $wR_2 = 0.1947$; 8479 independent reflections [$2\theta \leq 55.04^\circ$], and 417 parameters.

Crystal data of **5**. $\text{C}_{26}\text{H}_{34}\text{B}_6\text{MoO}_5\text{Rh}_2\text{S}_5$, formula weight, $M_r = 953.45$, orthorhombic, $Pbcn$, unit cell, $a = 18.0346(10) \text{ \AA}$, $b = 15.4968(12) \text{ \AA}$, $c = 27.550(2) \text{ \AA}$, $\alpha = 90^\circ$, $\beta = 90^\circ$, $\gamma = 90^\circ$; $Z = 8$; $V = 7699.6(9) \text{ \AA}^3$; $\mu = 1.471 \text{ mm}^{-1}$; $F(000) = 3776$; $\rho_{\text{calcd}} = 1.645 \text{ g/cm}^3$; $R_1 = 0.0422$; $wR_2 = 0.0969$; 8750 independent reflections [$2\theta \leq 54.99^\circ$], and 428 parameters.

Crystal data of **6**. $\text{C}_{26}\text{H}_{34}\text{B}_6\text{O}_5\text{Rh}_2\text{S}_5\text{W}$, formula weight, $M_r = 1041.36$, orthorhombic, $Pbcn$, unit cell, $a = 18.0153(15) \text{ \AA}$, $b = 15.5395(16) \text{ \AA}$, $c = 27.555(3) \text{ \AA}$, $\alpha = 90^\circ$, $\beta = 90^\circ$, $\gamma = 90^\circ$; $Z = 8$; $V = 7714.0(13) \text{ \AA}^3$; $\mu = 4.124 \text{ mm}^{-1}$; $F(000) = 4032$; $\rho_{\text{calcd}} = 1.793 \text{ g/cm}^3$; $R_1 = 0.0219$; $wR_2 = 0.0494$; 8770 independent reflections [$2\theta \leq 54.99^\circ$], and 428 parameters.

Crystal data of **7**. $\text{C}_{39}\text{H}_{36}\text{B}_6\text{Co}_2\text{O}_{18}\text{Ru}_7\text{S}_5$, $2(\text{CH}_2\text{Cl}_2)$, formula weight, $M_r = 2013.04$, triclinic, $P-1$, unit cell, $a = 11.6527(14) \text{ \AA}$, $b = 13.0484(12) \text{ \AA}$, $c = 21.925(2) \text{ \AA}$, $\alpha = 94.971(4)^\circ$, $\beta = 105.005(5)^\circ$, $\gamma = 99.109(5)^\circ$; $Z = 2$; $V = 3150.8(6) \text{ \AA}^3$; $\mu = 2.539 \text{ mm}^{-1}$; $F(000) = 1940$; $\rho_{\text{calcd}} = 2.122 \text{ g/cm}^3$; $R_1 = 0.0559$; $wR_2 = 0.1293$; 14194 independent reflections [$2\theta \leq 54.97^\circ$], and 758 parameters.

Crystal data of **8**. $\text{C}_{33}\text{H}_{34}\text{B}_6\text{Co}_6\text{O}_{13}\text{Rh}_2\text{S}_5$, formula weight, $M_r = 1423.16$, Triclinic, $P-1$, unit cell, $a = 12.4725(4) \text{ \AA}$, $b = 14.4351(5) \text{ \AA}$, $c = 16.0368(5) \text{ \AA}$, $\alpha = 88.7070(10)^\circ$, $\beta = 74.7360(10)^\circ$, $\gamma = 79.9110^\circ$; $Z = 2$; $V = 2741.52(16) \text{ \AA}^3$; $\mu = 2.594 \text{ mm}^{-1}$; $F(000) = 1396$; $\rho_{\text{calcd}} = 1.724 \text{ g/cm}^3$; $R_1 = 0.0295$; $wR_2 = 0.0764$; 13201 independent reflections [$2\theta \leq 56.00^\circ$], and 596 parameters.

3.7. Computational Details

All molecules were fully optimized using the BP86 functional [67,68], in conjunction with a def2-svp basis set using the Gaussian 16 program (Gaussian, Wallingford, CT, USA) [69]. All compounds were fully optimized in gaseous state using their X-ray crystallographic structures. The calculations were performed with the Cp analogues, instead of Cp^* , to save computing time. All the optimized structures and orbital graphics were produced using Gaussview [70] and Chemcraft [71].

4. Conclusions

In summary, we have synthesized and structurally characterized numerous exciting clusters 3–6 in which the S atom of the $\{B_2CS_3\}$ moiety is coordinated to group 6 metal carbonyl fragments in η^1 -fashion. On the other hand, we have established the structures of clusters 7 and 8 having very characteristic and unusual fusion. The molecular structure of cluster 7 consists of a butterfly $\{Ru_3S\}$ moiety that is almost flat. Cluster 8 shows bicapped square pyramidal $\{Co_6S\}$ unit that is fused with a butterfly $\{Co_2S_2\}$ via a common $\{Co_2\}$ edge. Although both the clusters are of condensed types, the electron counts are very complex and they do not follow any of the cluster-counting rules, including Mingos' fusion formalism and Jemmis' mno rule.

Supplementary Materials: The following supporting information can be downloaded at: <https://www.mdpi.com/article/10.3390/molecules28030998/s1>, Figures S1–S4: Molecular structures and labelling diagrams of 4–8; Figures S5–S19: spectroscopic details of 3–6, Figures S20–S21: selected molecular orbitals of 7 and 8, Figures S22–S27: Optimized geometries of 4–8 [72–74].

Author Contributions: Conceptualization, K.K., S.S. and S.G.; methodology, K.K., S.S., R.M.P. and S.G. software, K.K. and S.S.; validation, S.G.; formal analysis, K.K., S.S., R.M.P. and A.R.; investigation, K.K., S.S., R.M.P., A.R., M.C. and T.R.; data curation, K.K., S.S. and A.R.; writing—original draft preparation, K.K., S.S. and S.G.; writing—review and editing, K.K., S.S. and S.G.; visualization, K.K. and S.S.; supervision, S.G.; project administration, S.G.; funding acquisition, S.G. All authors have read and agreed to the published version of the manuscript.

Funding: This work was supported by the SERB, Grant No. CRG/2019/001280, New Delhi, India and the Centre of Excellence on Molecular Materials and Functions under the Institution of Eminence scheme of IIT Madras.

Institutional Review Board Statement: Not applicable.

Informed Consent Statement: Not applicable.

Data Availability Statement: Supporting data reported can be found as Supplementary Materials.

Acknowledgments: K.K. and S.S. thank DST-INSPIRE for research fellowships. A.R. thanks IIT Madras for research fellowship. We are grateful to SC-XRD LAB, SAIF, IIT Madras for X-ray data collection and structure refinement for 8. Computational facilities of IIT Madras are gratefully acknowledged.

Conflicts of Interest: The authors declare no conflict of interest.

Sample Availability: Samples of the compounds are available from the authors upon request.

References

- Grimes, R.N. Transition Metal Metallocarboranes. In *Comprehensive Organometallic Chemistry II*; Abel, E.W., Stone, F.G.A., Wilkinson, G., Eds.; Pergamon Press, Inc.: Oxford, UK, 1995; Volume 1, pp. 373–430.
- Hosmane, N.S. (Ed.) *Boron Science: New Technologies and Applications*; CRC Press, Inc.: Boca Raton, FL, USA, 2011.
- Housecroft, C.E. Boron Atoms in Transition Metal Clusters. *Adv. Organomet. Chem.* **1991**, *33*, 1–50.
- Pathak, K.; Saha, K.; Ghosh, S. Nanovehicles and Boron Clusters. In *Fundamentals and Applications of Boron Chemistry*; Zhu, Y., Hosmane, N., Eds.; Elsevier, Inc.: Oxford, UK, 2022; Volume 2.
- Borthakur, R.; Mondal, B.; Nandi, P.; Ghosh, S. Hypoelectronic Isomeric Diiridaboranes $[(Cp^*Ir)_2B_6H_6]$: The “Rule-Breakers” ($Cp^* = \eta^5-C_5Me_5$). *Chem. Commun.* **2016**, *52*, 3199–3202. [[CrossRef](#)] [[PubMed](#)]
- De, A.; Zhang, Q.-F.; Mondal, B.; Cheung, L.F.; Kar, S.; Saha, K.; Varghese, B.; Wang, L.-S.; Ghosh, S. $[(Cp_2M)_2B_9H_{11}]$ ($M = Zr$ or Hf): Early Transition Metal ‘Guarded’ Heptaborane with Strong Covalent and Electrostatic Bonding. *Chem. Sci.* **2018**, *9*, 1976–1981. [[CrossRef](#)]
- Kar, S.; Bairagi, S.; Haridas, A.; Joshi, G.; Jemmis, E.D.; Ghosh, S. Hexagonal Planar $[B_6H_6]$ within a $[B_6H_{12}]$ Borate Complex: Structure and Bonding of $[(Cp^*Ti)_2(\mu-\eta^6:\eta^6-B_6H_6)(\mu-H)_6]$. *Angew. Chem. Int. Ed.* **2022**, *61*, e202208293.
- Lipscomb, W.N. *Boron Hydrides*; Dover Publications Inc.: Mineola, NY, USA, 2012.
- Grimes, R.N. *Carboranes*, 3rd ed.; Elsevier: Oxford, UK, 2016; pp. 929–944.
- Burke, A.; Ellis, D.; Giles, B.T.; Hodson, B.E.; Macgregor, S.A.; Rosair, G.M.; Welch, A.J. Beyond the Icosahedron: The First 13-Vertex Carborane. *Angew. Chem. Int. Ed.* **2003**, *42*, 225–228. [[CrossRef](#)] [[PubMed](#)]
- Kennedy, J.D. The Polyhedral Metallaboranes Part II. Metallaborane Clusters with Eight Vertices and More. *Prog. Inorg. Chem.* **1986**, *34*, 211–434.

12. Ghosh, S.; Rheingold, A.L.; Fehlner, T.P. Metallaboranes of the earlier transition metals. An arachno nine-vertex, nine-skeletal electron pair rhenaborane of novel shape: Importance of total vertex connectivities in such systems. *Chem. Commun.* **2001**, 895–896. [\[CrossRef\]](#)
13. Ghosh, S.; Beatty, A.M.; Fehlner, T.P. Synthesis and Characterization of Bicapped Hexagonal Bipyramidal 2,3-Cl₂-1,8-{Cp*Re}₂B₆H₄[(Cp*Re)₂(μⁿ-n⁶-1,2-B₆H₄Cl₂), Cp* = n⁵-C₅Me₅]: The Missing Link Connecting (p-2) Skeletal Electron Pair Hypoelectronic Rhenaboranes and 24-Valence Electron Triple-Decker Complexes. *J. Am. Chem. Soc.* **2001**, *123*, 9188–9189.
14. Zheng, F.; Yui, T.H.; Zhang, J.; Xie, Z. Synthesis and X-ray characterization of 15- and 16-vertex *closo*-carboranes. *Nat. Commun.* **2020**, *11*, 5943–5947. [\[CrossRef\]](#)
15. Kar, S.; Pradhan, A.N.; Ghosh, S. Polyhedral Metallaboranes and Metallacarboranes. In *Comprehensive Organometallic Chemistry IV*, 4th ed.; Parkin, G., Meyer, K., O'hare, D., Eds.; Elsevier: Amsterdam, The Netherlands, 2022; Volume 9, pp. 263–369.
16. Roy, D.K.; Anju, R.S.; Varghese, B.; Ghosh, S. Reactivity of Dirhodium Analogues of Octaborane-12 and Decaborane-14 towards Transition-Metal Moieties. *Organometallics* **2013**, *32*, 1964–1970. [\[CrossRef\]](#)
17. Bose, S.K.; Geetharani, K.; Ramkumar, V.; Varghese, B.; Ghosh, S. Chemistry of Vanadaboranes: Synthesis, Structures, and Characterization of Organovanadium Sulfide Clusters with Disulfido Linkage. *Inorg. Chem.* **2010**, *49*, 2881–2888. [\[CrossRef\]](#) [\[PubMed\]](#)
18. Geetharani, K.; Bose, S.K.; Sahoo, S.; Varghese, B.; Mobin, S.M.; Ghosh, S. Cluster expansion reactions of group 6 and 8 metallaboranes using transition metal carbonyl compounds of groups 7–9. *Inorg. Chem.* **2011**, *50*, 5824–5832. [\[CrossRef\]](#) [\[PubMed\]](#)
19. Mondal, B.; Bag, R.; Ghorai, S.; Bakthavachalam, K.; Jemmis, E.D.; Ghosh, S. Synthesis, Structure, Bonding, and Reactivity of Metal Complexes Comprising Diborane(4) and Diborene(2): [(Cp*Mo(CO)₂)₂(μ-η²:η²-B₂H₄)] and [(Cp*M(CO)₂)₂B₂H₂M(CO)₄], M=Mo,W. *Angew. Chem. Int. Ed.* **2018**, *57*, 8079–8083. [\[CrossRef\]](#)
20. Krishnamoorthy, B.S.; Thakur, A.; Chakrahari, K.K.V.; Bose, S.K.; Hamon, P.; Roisnel, T.; Kahlal, S.; Ghosh, S.; Halet, J.-F. Theoretical and Experimental Investigations on Hypoelectronic Heterodimetallaboranes of Group 6 Transition Metals. *Inorg. Chem.* **2012**, *51*, 10375–10383. [\[CrossRef\]](#)
21. Bose, S.K.; Geetharani, K.; Varghese, B.; Ghosh, S. Condensed Tantalaborane Clusters: Synthesis and Structures of [(Cp*Ta)₂B₅H₇(Fe(CO)₃)₂] and [(Cp*Ta)₂B₅H₉(Fe(CO)₃)₄]. *Inorg. Chem.* **2011**, *50*, 2445–2449. [\[CrossRef\]](#)
22. Bose, S.K.; Geetharani, K.; Sahoo, S.; Reddy, K.H.K.; Varghese, B.; Jemmis, E.D.; Ghosh, S. Synthesis, characterization, and electronic structure of new type of heterometallic boride clusters. *Inorg. Chem.* **2011**, *50*, 9414–9422. [\[CrossRef\]](#)
23. Bose, S.K.; Ghosh, S. Linked and Fused Tungstaborane Clusters: Synthesis, Characterization, and Electronic Structures of bis-(η⁵-C₅Me₅W)₂B₅H₈ and (η⁵-C₅Me₅W)₂[Fe(CO)₃]_nB_{6-n}H_{10-n}, n = 0, 1. *Organometallics* **2007**, *26*, 5377–5385. [\[CrossRef\]](#)
24. Zafar, M.; Kar, S.; Nandi, C.; Ramalakshmi, R.; Ghosh, S. Cluster fusion: Face-fused macropolyhedral tetracobaltaboranes. *Inorg. Chem.* **2019**, *58*, 47–51. [\[CrossRef\]](#)
25. Geetharani, K.; Krishnamoorthy, B.S.; Kahlal, S.; Mobin, S.M.; Halet, J.-F.; Ghosh, S. Synthesis and Characterization of Hypoelectronic Tantalaboranes. Comparison of the Geometric and Electronic Structures of [(Cp*TaX)₂B₅H₁₁] (X = Cl, Br and I). *Inorg. Chem.* **2012**, *51*, 10176–10184. [\[CrossRef\]](#)
26. Anju, R.S.; Saha, K.; Mondal, B.; Dorcet, V.; Roisnel, T.; Halet, J.-F.; Ghosh, S. Chemistry of Diruthenium Analogue of Pentaborane(9) With Heterocumulenes: Towards Novel Trimetallic Cubane-type Clusters. *Inorg. Chem.* **2014**, *53*, 10527–10535. [\[CrossRef\]](#)
27. Roy, D.K.; Mondal, B.; Shankhari, P.; Anju, R.S.; Geetharani, K.; Mobin, S.M.; Ghosh, S. Supraicosahedral Polyhedra in Metallaboranes: Synthesis and Structural Characterization of 12-, 15- and 16-Vertex Rhodaboranes. *Inorg. Chem.* **2013**, *52*, 6705–6712. [\[CrossRef\]](#) [\[PubMed\]](#)
28. Roy, D.K.; Barik, S.K.; Mondal, B.; Varghese, B.; Ghosh, S. A Novel Heterometallic μ⁹-Boride Cluster: Synthesis and Structural Characterization of [(η⁵-C₅Me₅Rh)₂(Co₆(CO)₁₂)(μ-H)(BH)B]. *Inorg. Chem.* **2014**, *53*, 667–669. [\[CrossRef\]](#) [\[PubMed\]](#)
29. Zhang, X.; Yan, H. Transition metal-induced B–H functionalization of *o*-carborane. *Coord. Chem. Rev.* **2019**, *378*, 466–482. [\[CrossRef\]](#)
30. Hosmane, N.S.; Maguire, J.A. Metallacarboranes of d- and f-Block metals. In *Comprehensive Organometallic Chemistry III*; Crabtree, R.H., Mingos, D.M.P., Eds.; Elsevier: Oxford, UK, 2006.
31. Yao, Z.-J.; Huo, X.-K.; Jin, G.-X. Zwitterionic half-sandwich Rh and Ir complexes containing a diphosphine *nido*-carborane ligand: Synthesis, structure transformation and application in H₂ activation. *Chem. Commun.* **2012**, *48*, 6714–6716. [\[CrossRef\]](#)
32. Saha, K.; Roy, D.K.; Dewhurst, R.D.; Ghosh, S.; Braunschweig, H. Recent Advances in the Synthesis and Reactivity of Transition Metal σ-Borane/Borate Complexes. *Acc. Chem. Res.* **2021**, *54*, 1260–1273. [\[CrossRef\]](#)
33. Borthakur, R.; Saha, K.; Kar, S.; Ghosh, S. Recent advances in transition metal diborane(6), diborane(4) and diborene(2) chemistry. *Coord. Chem. Rev.* **2019**, *399*, 213021–213037. [\[CrossRef\]](#)
34. Grimes, R.N. Cluster forming and cage fusion in metallacarborane chemistry. *Coord. Chem. Rev.* **1995**, *143*, 71–96. [\[CrossRef\]](#)
35. Ghosh, S.; Noll, B.C.; Fehlner, T.P. Expansion of iridaborane clusters by addition of monoborane. Novel metallaboranes and mechanistic detail. *Dalton Trans.* **2008**, 371–378. [\[CrossRef\]](#)
36. Dhayal, R.S.; Sahoo, S.; Reddy, K.H.K.; Mobin, S.M.; Jemmis, E.D.; Ghosh, S. Vertex-Fused Metallaborane Clusters: Synthesis, Characterization and Electronic Structure of [(η⁵-C₅Me₅Mo)₃MoB₉H₁₈]. *Inorg. Chem.* **2010**, *49*, 900–904. [\[CrossRef\]](#)

37. Londesborough, M.G.S.; MacLean, E.J.; Teat, S.J.; Thornton-Pett, M.; Kennedy, J.D. Macropolyhedral boron-containing cluster chemistry. Synchrotron X-ray structural analysis of $[(\text{PMe}_2\text{Ph})_2\text{Pd}_2\text{B}_{16}\text{H}_{20}(\text{PMe}_2\text{Ph})_2]$ and $[(\text{PMe}_2\text{Ph})_3\text{Pt}_2\text{B}_{16}\text{H}_{18}(\text{PMe}_2\text{Ph})]$: Models of intermediates to more condensed metallaboranes from the $[(\text{PMe}_2\text{Ph})_2\text{PtB}_8\text{H}_{12}]$ thermolysis system. *Chem. Commun.* **2005**, 1584–1586. [\[CrossRef\]](#)
38. Barton, L.; Bould, J.; Kennedy, J.D.; Rath, N.P. Macropolyhedral boron-containing cluster chemistry. Isolation and characterisation of the eighteen-vertex *nido*-5'-iridaoctaborano $[3',8':1',2]$ -closo-4-iridadodecaborane, $[(\text{CO})(\text{PMe}_3)_2\text{IrB}_{16}\text{H}_{14}\text{Ir}(\text{CO})(\text{PMe}_3)_2]$. *J. Chem. Soc. Dalton Trans.* **1996**, 3145–3149. [\[CrossRef\]](#)
39. Ghosh, S.; Lei, X.; Shang, M.; Fehlner, T.P. Role of the Transition Metal in Metallaborane Chemistry. Reactivity of $(\text{Cp}^*\text{ReH}_2)_2\text{B}_4\text{H}_4$ with $\text{BH}_3\cdot\text{thf}$, CO, and $\text{Co}_2(\text{CO})_8$. *Inorg. Chem.* **2000**, 39, 5373–5382. [\[CrossRef\]](#) [\[PubMed\]](#)
40. Ghosh, S.; Fehlner, T.P.; Noll, B.C. Condensed metallaborane clusters: Synthesis and structure of $\text{Fe}_2(\text{CO})_6(\eta^5\text{-C}_5\text{Me}_5\text{RuCO})(\eta^5\text{-C}_5\text{Me}_5\text{Ru})\text{B}_6\text{H}_{10}$. *Chem. Commun.* **2005**, 3080–3082. [\[CrossRef\]](#) [\[PubMed\]](#)
41. Ghosh, S.; Shang, M.; Fehlner, T.P. A Novel Coordinated Inorganic Benzene: Synthesis and Characterization of $\{\eta^5\text{-C}_5\text{Me}_5\text{Re}\}_2\{\mu\text{-}\eta^6\text{-}\eta^6\text{-B}_4\text{H}_4\text{Co}_2(\text{CO})_5\}$. *J. Am. Chem. Soc.* **1999**, 121, 7451–7452. [\[CrossRef\]](#)
42. Nandi, C.; Kar, K.; Gayen, S.; Roisnel, T.; Ghosh, S. Directed Synthesis of CS_2 and CS_3 -Bridged Decaborane-14 Analogues. *Inorg. Chem.* **2021**, 60, 12367–12376. [\[CrossRef\]](#)
43. Nandi, C.; Roy, A.; Kar, K.; Cordier, M.; Ghosh, S. Cluster Growth Reactions: Structures and Bonding of Metal-Rich Metallaheteroboranes Containing Heavier Chalcogen Elements. *Inorg. Chem.* **2022**, 61, 16750–16759. [\[CrossRef\]](#)
44. Pathak, K.; Nandi, C.; Ghosh, S. Metallaheteroboranes with group 16 elements: Aspects of synthesis, framework and reactivity. *Coord. Chem. Rev.* **2022**, 453, 214303–214331. [\[CrossRef\]](#)
45. Nandi, C.; Kar, S.; Zafar, M.; Kar, K.; Roisnel, T.; Dorcet, V.; Ghosh, S. Chemistry of Dimetalla-octaborane(12) with Chalcogen-Based Borate Ligands: Obedient versus Disobedient Clusters. *Inorg. Chem.* **2020**, 59, 3537–3541. [\[CrossRef\]](#)
46. Sahoo, S.; Mobin, S.M.; Ghosh, S. Direct Insertion of Sulphur, Selenium and Tellurium atoms into Metallaborane Cages using Chalcogen Powders. *J. Organomet. Chem.* **2010**, 695, 945–949. [\[CrossRef\]](#)
47. Baird, M.C.; Wilkinson, G. Bis(triphenylphosphine)(carbon disulphide)platinum. *Chem. Commun.* **1966**, 514–515. [\[CrossRef\]](#)
48. Vicente, J.; Chicote, M.T.; González-Herrero, P.; Jones, P.G.J. Synthesis of the first trithiocarbonatogold complex: $[\text{N}(\text{PPh}_3)_2]_2[\text{Au}_2(\mu^2\text{-}\eta^2\text{-CS}_3)_2]$. First crystal structure of a $\mu^2\text{-}\eta^2$ -bridging trithiocarbonato complex. *Chem. Soc. Chem. Commun.* **1995**, 745–746. [\[CrossRef\]](#)
49. Zhong, M.; Zhang, J.; Lu, Z.; Xie, Z. Diboration of Alkenes and Alkynes with a Carborane-Fused Four-Membered Boracycle Bearing an Electron-Precise B-B Bond. *Dalton Trans.* **2021**, 50, 17150–17155. [\[CrossRef\]](#) [\[PubMed\]](#)
50. Bianchini, C.; Mealli, C.; Meli, A.; Scapacci, G. Cobalt(II) and nickel(II) trithiocarbonate complexes as nucleophilic reagents. Reactivity and X-ray structure of the trithiocarbonate complex $[\text{Co}(\text{tppme})(\text{S}_2\text{CSCH}_3)][\text{BPh}_4]\cdot 1.5\text{thf}$. *J. Chem. Soc. Dalton Trans.* **1982**, 799–804. [\[CrossRef\]](#)
51. Gill, D.S.; Green, M.; Marsden, K.; Moore, I.; Orpen, A.G.; Stone, F.G.A.; Williams, I.D.; Woodward, P. The reaction of molybdenum and tungsten carbyne complexes with sulphur and selenium; crystal structures of $[\text{Mo}\{\eta^2\text{-(S}_2\text{CCH}_2\text{But)}\}(\text{CO})_2(\eta\text{-C}_5\text{H}_5)]$ and $[\text{W}\{\eta^2\text{-(S}_2\text{CC}_6\text{H}_4\text{Me-4)}\}(\text{CO})_2(\eta\text{-C}_5\text{H}_5)]$. *J. Chem. Soc. Dalton Trans.* **1984**, 1343–1347. [\[CrossRef\]](#)
52. Kar, S.; Kar, K.; Ghosh, S. Vertex-Fused Clusters Featuring a Flattened Butterfly. *Organometallics* **2022**, 41, 1125–1129. [\[CrossRef\]](#)
53. Saha, K.; Kaur, U.; Kar, S.; Mondal, B.; Joseph, B.; Antharjanam, P.K.S.; Ghosh, S. Trithia-diborinane and Bis(bridging-boryl) Complexes of Ruthenium Derived from a $[\text{BH}_3(\text{SCH}_3)]^-$ Ion. *Inorg. Chem.* **2019**, 58, 2346–2353. [\[CrossRef\]](#)
54. Saha, K.; Gayen, S.; Kaur, U.; Roisnel, T.; Ghosh, S. Stabilization of dichalcogenide ligands in the coordination sphere of a ruthenium system. *Dalton Trans.* **2021**, 50, 12990–13001. [\[CrossRef\]](#)
55. Kaur, P.; Thornton-Pett, M.; Clegg, W.; Kennedy, J.D. Macropolyhedral boron-containing cluster chemistry: Nineteen-vertex $[(\text{PPh}_3)\text{NiS}_2\text{B}_{16}\text{H}_{12}(\text{PPh}_3)]$ and eighteen-vertex $\text{S}_2\text{B}_{16}\text{H}_{14}(\text{PPh}_3)$. *J. Chem. Soc. Dalton Trans.* **1996**, 1996, 4155–4157. [\[CrossRef\]](#)
56. Wade, K. The Structural Significance of the Number of Skeletal Bonding Electron-Pairs in Carboranes, the Higher Boranes and Borane Anions, and Various Transition-Metal Carbonyl Cluster Compounds. *J. Chem. Soc. D* **1971**, 792–793. [\[CrossRef\]](#)
57. Wade, K. Structural and Bonding Patterns in Cluster Chemistry. *Adv. Inorg. Chem. Radiochem.* **1976**, 18, 1–66.
58. Mingos, D.M.P. Polyhedral Skeletal Electron Pair Approach. *Acc. Chem. Res.* **1984**, 17, 311–319. [\[CrossRef\]](#)
59. Jemmis, E.D.; Balakrishnarajan, M.M.; Pancharatna, P.D. Electronic Requirements for Macropolyhedral Boranes. *Chem. Rev.* **2002**, 102, 93–144. [\[CrossRef\]](#) [\[PubMed\]](#)
60. Sheldrick, G.M. SHELXT—Integrated space-group and crystal-structure determination. *Acta Cryst.* **2015**, A71, 3–8. [\[CrossRef\]](#)
61. Sheldrick, G.M. SHELXS97 and SHELXL97. Program for Crystal Structure Solution and Refinement; University of Gottingen: Gottingen, Germany, 1997.
62. Sheldrick, G.M. SHELXT—Crystal structure refinement with SHELXL. *Acta Cryst.* **2015**, C71, 3–8.
63. Van der Sluis, P.; Spek, A.L. BYPASS: An effective method for the refinement of crystal structures containing disordered solvent regions. *Acta Cryst.* **1990**, A46, 194–201. [\[CrossRef\]](#)
64. Spek, A.L. Single-crystal structure validation with the program PLATON. *J. Appl. Cryst.* **2003**, 36, 7–13. [\[CrossRef\]](#)
65. Spek, A.L. Structure validation with the program PLATON. *Acta Cryst.* **2009**, D65, 148–155.
66. Dolomanov, O.V.; Bourhis, L.J.; Gildea, R.J.; Howard, J.A.K.; Puschmann, H. OLEX2: A complete structure solution, refinement and analysis program. *J. Appl. Crystallogr.* **2009**, 42, 339–341. [\[CrossRef\]](#)

67. Schmider, H.L.; Becke, A.D. Optimized density functionals from the extended G2 test set. *J. Chem. Phys.* **1998**, *108*, 9624–9631. [CrossRef]
68. Perdew, J.P. Density-functional approximation for the correlation energy of the inhomogeneous electron gas. *Phys. Rev. B* **1986**, *33*, 8822–8824. [CrossRef]
69. Frisch, M.J.; Trucks, G.W.; Schlegel, H.B.; Scuseria, G.E.; Robb, M.A.; Cheeseman, J.R.; Scalmani, G.; Barone, V.; Petersson, G.A.; Nakatsuji, H.; et al. *Gaussian 16, Revision B.01*; Gaussian, Inc.: Wallingford, CT, USA, 2016.
70. Dennington, I.I.; Keith, R.T.; Millam, J.; Eppinnett, K.; Hovell, W.L.; Gilliland, R. *GaussView, Version 3.09*; Semichem Inc.: Shawnee, KS, USA, 2003.
71. Chemcraft—Graphical Software for Visualization of Quantum Chemistry Computations. Available online: <https://www.chemcraftprog.com> (accessed on 7 October 2022).
72. Led, J.J.; Gesmar, H. Application of the linear prediction method to NMR spectroscopy. *Chem. Rev.* **1991**, *91*, 1413–1426. [CrossRef]
73. Yang, L.; Simionescu, R.; Lough, A.; Yan, H. Some observations relating to the stability of the BODIPY fluorophore under acidic and basic conditions. *Dyes Pigm.* **2011**, *91*, 264–267. [CrossRef]
74. Weiss, R.; Grimes, R.N. Sources of Line Width in Boron-11 Nuclear Magnetic Resonance Spectra. Scalar Relaxation and Boron-Boron Coupling in B₄H₁₀ and B₅H₉. *J. Am. Chem. Soc.* **1978**, *100*, 1401–1405. [CrossRef]

Disclaimer/Publisher’s Note: The statements, opinions and data contained in all publications are solely those of the individual author(s) and contributor(s) and not of MDPI and/or the editor(s). MDPI and/or the editor(s) disclaim responsibility for any injury to people or property resulting from any ideas, methods, instructions or products referred to in the content.